Assessing Body Thermoregulation under Localized Cold Stress Using MWIR and LWIR Thermography

by Fumin Wang[1,2], Clemente Ibarra-Castanedo[2,3], Francesco Giardini[2], Xavier Maldague[3], Yi Liu[1*], Yuan Yao[4*], Stefano Sfarra[2]

[1] *Institute of Process Equipment and Control Engineering, Zhejiang University of Technology, Hangzhou, China*

[2] *Department of Industrial and Information Engineering and Economics, University of L'Aquila, L'Aquila, Italy*

[3] *Department of Electrical and Computer Engineering, Laval University, Quebec, Canada*

[4] *Department of Chemical Engineering, National Tsing Hua University, Hsinchu, Taiwan*

Abstract

Abnormal body temperature is an important indicator of physiological health and thermoregulatory function. Infrared thermography (IRT) provides a rapid, passive, non-contact and non-invasive method for monitoring body surface temperature. Unlike conventional thermometers, IRT enables remote visualization and quantitative analysis of spatial thermal patterns and their dynamic changes. This study used MWIR/LWIR IRT to investigate bilateral hand thermal responses under localized cold stimulation. Nineteen volunteers underwent 4 minutes of right-hand cold exposure at −4°C followed by 4 minutes of recovery, while both hands were continuously imaged. Regions of interest were analysed using principal component thermography and deep autoencoder to enhance visualization of the ventral plexus. Results showed continuous cooling and subsequent recovery in the stimulated hand, accompanied by warming in the unstimulated hand. These findings suggest that localized cold stress induces cross-limb vasomotor coupling and systemic thermal redistribution.

1. Introduction

The maintenance of human thermal homeostasis depends on precise neurovascular regulation and the dynamic balance between thermogenesis and heat dissipation. Even under substantial fluctuations in ambient temperature, the human body can preserve a relatively stable core temperature through peripheral vasomotor regulation, redistribution of blood flow, and autonomic nervous control, thereby supporting vital organ function and overall physiological homeostasis [1-3]. As a peripheral region with a dense vascular network and high thermal sensitivity, the hand provides an important anatomical site for investigating both local and systemic thermoregulatory responses to cold stimulation.

Infrared thermography (IRT) [4-6] offers the advantages of being non-contact, real-time, and capable of two-dimensional visualization, enabling continuous monitoring of skin surface temperature fields. It has therefore become a valuable tool for assessing peripheral circulation, vasomotor responses, and thermoregulatory processes. In recent years, mid-wave infrared and long-wave IRT have been increasingly applied in biomedical inspection, blood perfusion assessment, and the analysis of cold-induced thermal responses [7]. However, hand temperature distribution is influenced by multiple factors, including individual variability, vascular architecture, local tissue properties, and environmental conditions. During dynamic cold stimulation, conventional temperature analysis methods remain limited in identifying low-contrast vascular thermal features, extracting temperature variation patterns in key regions, and revealing thermoregulatory coupling between bilateral limbs.

Principal component thermography (PCT) [8-10] is an effective method for analysing thermal image sequences. By performing dimensionality reduction and feature enhancement, it can extract dominant patterns of temperature variation and highlight key information associated with vascular distribution and heat transfer. Meanwhile, deep learning methods have shown considerable potential in medical image enhancement, feature extraction, and complex pattern recognition. Deep autoencoder (DAT) [11, 12] can learn latent nonlinear representations from thermal images, helping to reduce noise interference and improve the stability and accuracy of infrared thermographic analysis. Therefore, integrating principal component thermography with DAT-based analysis may provide more reliable technical support for vascular region localization and dynamic thermal response assessment in infrared thermographic sequences.

In this study, mid-wave and long-wave IRT were employed to continuously capture dorsal temperature field variations of both hands under localized cold stimulation. During the experiment, cold stimulation was applied to the volar surface of the right hand, while thermal responses of both the stimulated and unstimulated hands were simultaneously recorded during the cold exposure and recovery phases. By combining region-of-interest analysis, principal component thermography, and a DAT method, this study characterizes the dynamic temperature changes in regions associated with the volar vascular plexus and further investigates bilateral thermal redistribution and potential

cross-limb vasomotor coupling induced by localized cold stress. The findings provide experimental evidence for understanding peripheral thermoregulation and systemic thermal redistribution in the human body.

2. Data Acquisition

Thermographic data acquisition was performed in a controlled examination room to minimize environmental interference and background infrared radiation. Before the measurement, each participant was invited into the room and instructed to sit quietly in preparation for the experimental protocol. The room was kept free from major infrared radiation sources, such as direct sunlight, active electronic devices, or other heat-emitting objects. The ambient temperature was maintained between 20°C and 26°C to avoid undesired thermoregulatory responses, since temperatures above this range may induce sweating, whereas lower temperatures may trigger shivering and consequently alter peripheral skin temperature.

After acclimatization, participants were asked to remove rings, bracelets, watches, and other accessories that might affect thermal measurements. They were also instructed to roll up their sleeves and position both hands above the examination table without touching it until the imaging system was ready. A metal slab, previously cooled in an ALPICOOL 60 W portable refrigerator, was then removed and placed on the examination table. The slab surface was coated with high-emissivity black paint to ensure a stable emissivity value and was cooled to approximately -4°C before testing. At the start of acquisition, the participant placed the right hand on the cold slab to receive localized cold stimulation, while the left hand was placed paper support at room temperature and served as the non-stimulated contralateral control. The paper support had the same thickness of the slab.

Thermal data were acquired using a bi-spectral infrared imaging system. A FLIR T1020 camera operating in the long-wave infrared range of 7-14 μm, with a resolution of 1024 × 786 pixels and a noise-equivalent temperature difference below 20 mK at 30°C, was used for LWIR imaging. Simultaneously, a cooled FLIR A6700 camera operating in the mid-wave infrared range of 3-5 μm, with a resolution of 640 × 512 pixels and a noise-equivalent temperature difference below 20 mK at 30°C, was used for MWIR imaging. Both cameras were mounted on MANFROTTO 055 tripods to ensure stable acquisition. The object-to-camera distance was fixed at 1 m for all measurements, and the skin emissivity was set to 0.98 according to values commonly used in human thermographic studies. The specific arrangement of the experimental equipment and hand positions are shown in Figure 1.

Figure 1. Experimental data acquisition equipment and hand positions

The standard acquisition protocol lasted approximately 8 minutes and consisted of two consecutive phases. During the first 4 minutes, cold stress was applied to the right hand through direct contact with the cooled metal slab, while the left hand remained on the room-temperature journal. Thermal images of both hands were continuously recorded during this period. After the cold-stimulation phase, recording was briefly stopped, and the participant was asked to slowly raise both hands while keeping them as still as possible. The cold slab was then removed, cleaned to eliminate sweat or residual fluids, and returned to the refrigerator for subsequent use. A second room-temperature paper support was placed in the original position of the slab, after which the participant lowered both hands onto the journals. The recovery phase was then recorded for an additional 4 minutes.

Both cameras were generally operated at a frame rate of 10 Hz, enabling continuous monitoring of dynamic temperature changes throughout the stimulation and recovery phases. In selected cases, longer recordings lasting 5–12 minutes were performed at 5 Hz to further investigate delayed thermal inversion responses. For subsequent analysis, four vein pixels were selected from vascular regions on the dorsal surfaces of both hands, including two pixels from the stimulated right hand and two from the non-stimulated left hand. These data provided the basis for quantitative assessment of bilateral thermal responses induced by localized cold stimulation.

3. Data Analysis Methods

The acquired MWIR and LWIR thermal image sequences were processed independently to characterize the dynamic temperature response of the stimulated and non-stimulated hands. Each thermographic sequence was represented as a three-dimensional dataset, consisting of two spatial dimensions and one temporal dimension. Let $I_t(x,y)$ denote the temperature value at pixel position (x,y) in the t-th thermal frame, where $t=1,2,\ldots,N$, and N is the total number of acquired frames. For subsequent matrix-based analysis, each two-dimensional thermal frame was reshaped into a one-dimensional vector:

$$\mathbf{x}_t = \left[\Delta I_t(1), \Delta I_t(2), \cdots, \Delta I_t(M)\right] \in \mathbb{R}^M \tag{1}$$

where $M=H\times W$ is the total number of pixels in each thermal frame. H and W represent the height and width of the image, respectively. The complete thermal sequence was arranged into a data matrix:

$$\mathbf{X} = \begin{bmatrix} \mathbf{x}_1 \\ \mathbf{x}_2 \\ \vdots \\ \mathbf{x}_N \end{bmatrix} \in \mathbb{R}^{N\times M} \tag{2}$$

where each row corresponds to one thermal frame and each column corresponds to the temporal evolution of one pixel.

3.1. Principal Component Thermography

Principal component thermography was applied to extract dominant spatial and temporal thermal variation patterns from the infrared image sequences. PCT is based on principal component analysis and transforms the original correlated thermal data into a set of orthogonal components. These components can highlight subtle thermal structures, such as vascular-related temperature patterns, that may be difficult to identify in raw thermographic images. Before decomposition, the data matrix was mean-cantered:

$$\tilde{\mathbf{X}} = \mathbf{X} - \overline{\mathbf{X}} \tag{3}$$

where $\overline{\mathbf{X}}$ represents the temporal mean of the thermal data matrix. After mean cantering, principal component decomposition was performed on the cantered matrix:

$$\tilde{\mathbf{X}} = \mathbf{U}\mathbf{\Sigma}\mathbf{V}^T \tag{4}$$

where **U** contains the temporal information, **Σ** is the singular value matrix, and **V** contains the dominant spatial feature patterns. The principal component images were obtained by reshaping the corresponding principal component vectors back to the original image dimensions:

$$PC_k = \mathrm{reshape}(\mathbf{v}_k) \tag{5}$$

where PC_k denotes the k-th principal component image, and $\mathbf{v}k$ is the corresponding principal component vector. In this study, PCT was mainly used to enhance vascular-related thermal features in the infrared image sequences and to assist in the identification of regions of interest for subsequent temperature analysis.

3.2. Deep Autoencoder Thermography

To further improve the quality of thermographic analysis and enhance the extraction of nonlinear thermal features, a DAT analysis method was employed. In this study, this method is referred to as DAT. Unlike PCT, which is based on linear orthogonal decomposition, the DAT learns a nonlinear low-dimensional representation of thermal images through an encoder–decoder architecture.

For each thermal frame or selected image patch, the input vector was denoted as $\mathbf{x} \in \mathbb{R}^M$. The encoder maps the original high-dimensional thermal input into a latent feature representation:

$$\mathbf{z} = f_\theta(\mathbf{x}) \tag{6}$$

here, **z** denotes the latent feature vector, and $f_\theta(\cdot)$ represents the nonlinear encoder parameterized by θ. A typical multilayer encoder can be expressed as:

$$\mathbf{h}^{(l)} = \sigma\left(\mathbf{W}^{(l)}\mathbf{h}^{(l-1)} + \mathbf{b}^{(l)}\right), \quad l = 1, 2, \ldots, L \tag{7}$$

where $W^{(l)}$ and $b^{(l)}$ are the weight matrix and bias vector of the l-th layer, respectively, and $\sigma(\cdot)$ denotes the nonlinear activation function. The output of the last hidden layer of the encoder forms the latent feature representation:

$$\mathbf{z} = \mathbf{h}^{(L)} \tag{8}$$

The decoder reconstructs the thermal image input from the latent feature representation:

$$\mathbf{x} = g_\phi(\mathbf{z}) \tag{9}$$

where $g_\phi(\cdot)$ represents the decoder parameterized by ϕ, and $\mathbf{x}$ denotes the reconstructed thermal image vector. Therefore, the overall mapping relationship of the autoencoder can be written as:

$$\mathbf{x} = g_\phi\left(f_\theta(\mathbf{x})\right) \tag{10}$$

DAT analysis was employed to extract nonlinear latent features from the infrared thermal images. For each thermal image frame or selected image patch, the input was represented as a vector $\mathbf{x} \in \mathbb{R}^M$. The encoder mapped the high-dimensional thermal input into a lower-dimensional latent space, where the latent vector $\mathbf{z} \in \mathbb{R}^d$ satisfied $d<M$. Through multiple nonlinear transformations, the encoder progressively extracted representative thermal features, and the output of the final hidden layer was regarded as the latent representation. Subsequently, the decoder reconstructed the thermal image from this latent representation. The overall autoencoder therefore learned a nonlinear mapping from

the original thermal image to its reconstructed representation, enabling noise suppression and feature enhancement in the thermographic data.

4. Experiment

This study aimed to visualize the temperature field of the dorsal surface of the hand using IRT and to quantitatively characterize bilateral thermal responses and systemic thermoregulatory adjustments induced by localized cold stimulation. A total of 19 healthy participants were enrolled, including 13 males and 6 females, aged 18–53 years. Among them, 17 participants exhibited a consistent thermal response pattern, indicating that comparable thermoregulatory behaviours could be identified across most individuals. Distinct temperature distribution patterns were observed in both the hand dorsum and fingers, suggesting that IRT can capture spatially heterogeneous thermal responses associated with peripheral thermoregulation.

Representative raw thermal images acquired during the experiment are shown in Figure 2. Owing to the continuous image acquisition protocol, many thermal images were generated for each participant. However, the direct identification of venous points (VPs) from raw thermographic images remains challenging because of the low thermal contrast, inter-individual anatomical variability, and noise introduced during image acquisition. Therefore, machine-learning-based image analysis is required to enhance VP localization and support subsequent quantitative assessment.

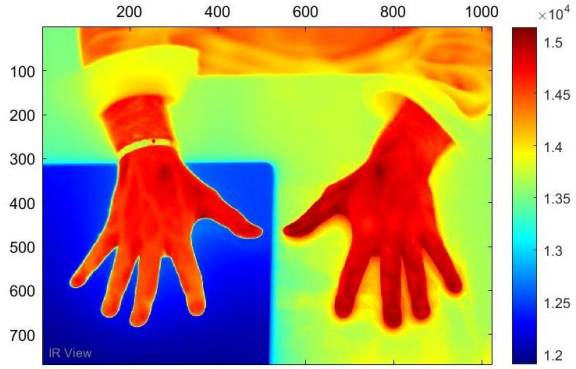

Figure 2. Visualization results of the original image

4.1. VP Selection Strategy

Figure 3 shows the principal component thermography (PCT)-processed images of the right hand under cold stimulation and the left hand maintained at room temperature. The venous-point (VP) distribution in the cold-stimulated hand was clearly visualized, indicating that PCT effectively enhanced the thermal contrast associated with superficial venous structures. In contrast, the VP in the hand under room-temperature conditions was less distinguishable, as the thermal features showed limited contrast against the surrounding background. In the sixth principal component image (PC6), the VP distribution of the cold-stimulated right hand could be clearly observed, whereas the VP pattern of the left hand remained partially incomplete.

To further improve VP identification, DAT was applied to extract representative features from the original thermal image sequences, as illustrated in Figure 4. By contrast, the DAT-derived feature maps provided enhanced visualization of the VP distribution. When interpreted together with the PCT results, the DAT features enabled more reliable localization of VPs in the cold-stimulated hand. Notably, in the latent-variable representations LV3 and LV6, the bilateral VP distributions became more apparent, allowing improved identification of venous thermal patterns in both hands. These findings suggest that the combination of PCT and DAT can enhance the extraction of subtle vascular thermal features.

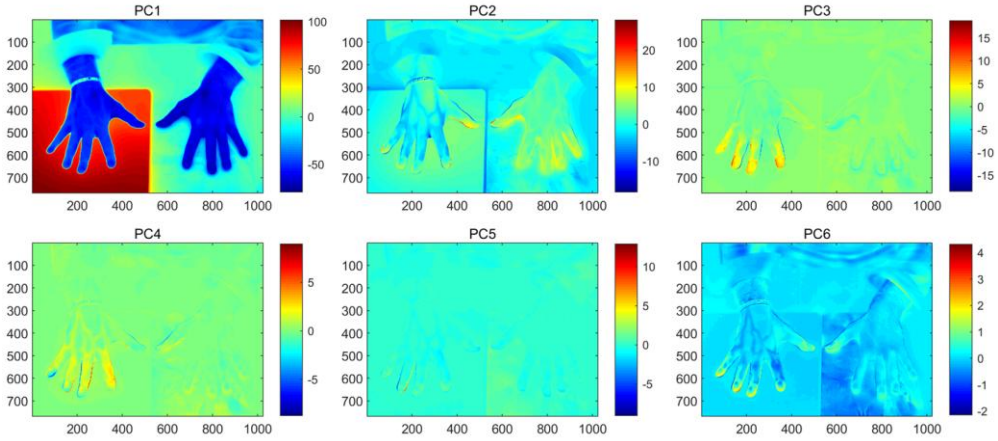

Figure 3. Visualization results of the PCT

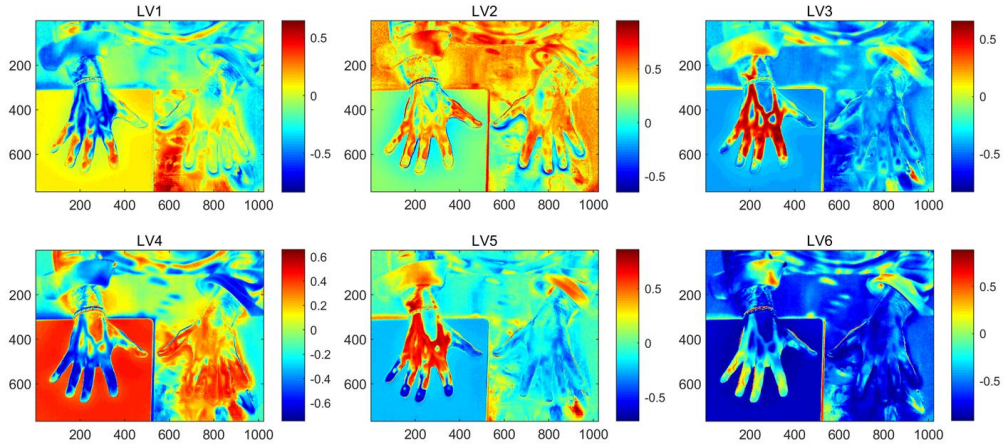

Figure 4. Visualization results of the DAT

4.2. Analysis of VP Changes

Following exposure of one hand to cold stimulation and maintenance of the contralateral hand at room temperature, the thermal distributions of both hands were examined immediately. As shown in Figure 5. The temperatures of the selected venous points (VPs) remained nearly stable during the first few seconds, suggesting an initial transient phase before detectable thermoregulatory responses emerged. After approximately 2 min, the VP temperature profiles in the cold-stimulated hand began to deviate from those in the non-stimulated hand. As shown in Figure 6.

In the cold-stimulated right hand, the temperatures of the selected VPs decreased progressively, consistent with cutaneous vasoconstriction and the consequent reduction in peripheral blood perfusion and convective heat transfer. Conversely, the selected VPs in the left hand exhibited a gradual temperature increase, indicating cutaneous vasodilation and enhanced heat transport from the body core to the skin surface. These opposing bilateral responses reveal a coordinated thermoregulatory mechanism by which localized cold stress elicits systemic vascular adjustments to maintain thermal homeostasis.

Figure 5. The condition of Subject 14's hands during cold stimulation

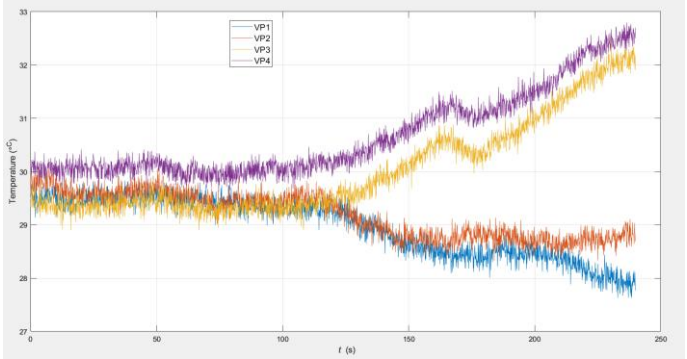

Figure 6. Temperature-time curve showing the temperature trend in the VP of Subject 14 under cold stimulation

Figure 7 present the thermographic responses recorded after removal of the cold stimulus. Immediately after stimulus withdrawal, the temperatures of the selected venous points (VPs) remained nearly stable for a short period. In 17 of the 19 participants, however, the temperatures of both hands subsequently began to increase after a characteristic delay, here defined as the "inversion time". This interval ranged from 10 s to 2 min, with an average duration of approximately 1 min.

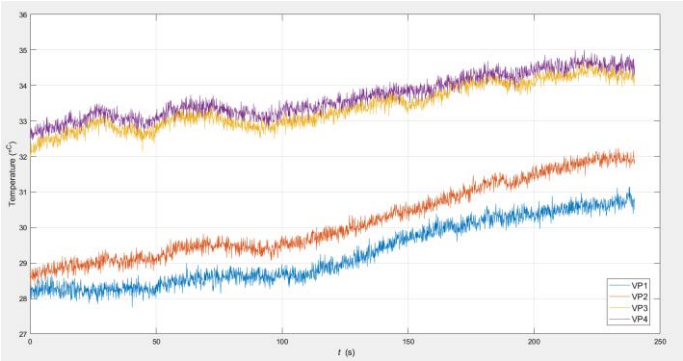

Figure 7. Temperature-time curve showing the temperature trend in the VP of Subject 14 cold stimulation

During this phase, the cold-stimulated right hand shifted from cutaneous vasoconstriction to vasodilation, indicating recovery of peripheral blood perfusion after cold exposure. In contrast, the contralateral hand exhibited no marked change in vascular state. The recovery process continued until a stable thermal condition was reached, suggesting that thermoregulatory adjustment ceased once peripheral temperature balance had been restored.

As clearly illustrated in Figures 8, the onset of vasodilation in the right hand was associated with a progressive increase in VP temperature, which gradually approached a subject-specific equilibrium level. These results indicate that removal of localized cold stress induces a delayed vascular recovery response, providing further evidence of dynamic peripheral thermoregulation.

4.3. Focus on Particular Behaviours

Subjects 4 and 18 showed atypical thermal response patterns relative to the remaining participants. In most subjects, the reversal of vasoconstriction was observed approximately 1 minute after the cold plate was removed. However, these two subjects exhibited a shift from cold-induced vasoconstriction to vasodilation while the cold stimulus was still present. This response indicates an accelerated thermoregulatory adjustment under sustained localized cooling.

Subject 18 completed the standard 8-min protocol, whereas subject 4 voluntarily underwent an extended 12-min recording in which the cold plate was continuously maintained beneath the right hand. The extended protocol was designed to further examine the inversion phenomenon and to characterize the vascular response elicited by prolonged cold exposure.

For subject 18, Figure 8 shows the processed thermographic images of the cold-stimulated right hand and the contralateral left hand maintained at room temperature, while Figure 9 presents the temporal evolution of the selected VPs. During the initial phase, VP temperatures in both hands remained relatively stable. Shortly after 1 min, however, all selected VPs exhibited a marked temperature increase, despite continued contact between the right hand and the cold plate. This indicates that vasodilation was initiated before removal of the cold stimulus.

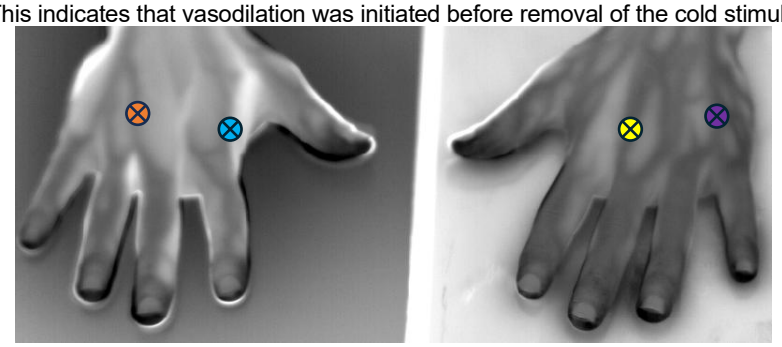

Figure 8. The condition of Subject 18's hands during cold stimulation

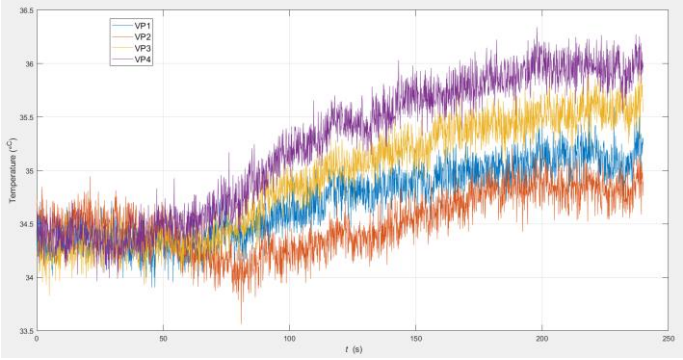

Figure 9. Temperature-time curve showing the temperature trend in the VP of Subject 18 under cold stimulation

Both subjects shared a high level of regular physical training. Subject 4 reported intensive exercise at least four times per week, regular aerobic training, and strict dietary habits aimed at maintaining muscle mass. Subject 18 similarly reported training three to four times per week, regular aerobic exercise, and a diet designed to preserve muscle mass. Although other participants also reported generally healthy lifestyles, the training intensity and consistency of subjects 4 and 18 were considered substantially above the cohort average. These observations suggest that enhanced physical conditioning may be associated with faster peripheral vascular adjustment and more efficient thermoregulatory recovery.

Figure 10 shows the temperature-time curve after the cold stimulus was removed. Once the cold plate was removed from beneath the subject's right hand, the hand was monitored under room-temperature conditions. The temperatures of all selected VPs remained relatively stable during the initial recovery phase, apart from minor oscillations.

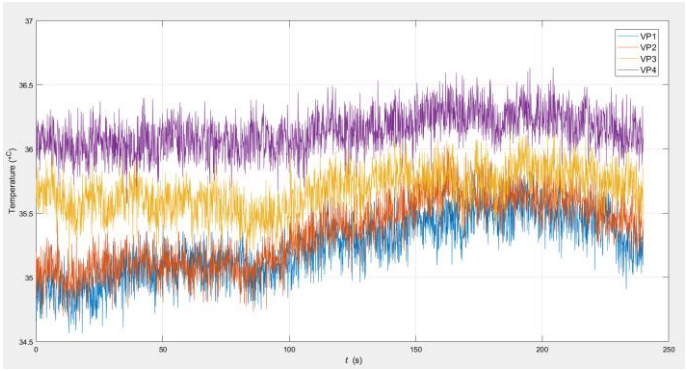

Figure 10. Temperature-time curve showing the temperature trend in the VP of Subject 18 after cold stimulation

Compared with less physically active participants, this subject showed more comparable thermal profiles between the two hands, indicating a more balanced bilateral thermoregulatory response. After approximately 1 min 30 s, the stable temperature pattern began to shift, with a slight increase in VP temperature subsequently observed. This delayed temperature rise suggests ongoing vascular recovery and peripheral thermoregulatory adjustment after withdrawal of the cold stimulus.

5. Conclusion

This study demonstrates that MWIR/LWIR IRT, combined with PCT and DAT, enables non-contact visualization and quantitative assessment of bilateral hand thermoregulatory responses under localized cold stimulation. The proposed PCT-DAT framework enhanced vascular thermal features and improved VP identification from raw thermographic sequences. Cold stimulation of the right hand at −4 °C produced progressive VP cooling, whereas the contralateral hand showed gradual warming, reflecting cutaneous vasoconstriction, compensatory vasodilation and systemic heat redistribution. Following stimulus removal, the stimulated hand exhibited delayed rewarming, with an average inversion time of approximately 1 min in most participants. These results indicate that localized cold stress induces coordinated bilateral vascular regulation. Larger studies with repeated stimulation protocols are needed to further investigate individual differences in peripheral vascular and thermoregulatory function.

Notes:

All IRT analyses for this experiment were conducted at the Department of Industrial and Information Engineering and Economics at the University of L'Aquila.

Acknowledgements

Yi Liu was supported in part by the National Natural Science Foundation of China (Grant No. U23A20328). Dr. Clemente Ibarra-Castanedo was supported by the DIIIE-UNIVAQ under Grant CA.04.01.02.04 (Hospitality and visiting professors, experts, speakers at conferences and seminars). Yuan Yao was supported in part by the National Science and Technology Council, Taiwan, under Project NSTC 114-2218-E-007-018. Fumin Wang was supported by the 2025 Postgraduate Internationalization Training Special Fund (Grant No. GF25034135001).

References

[1] Lahiri B B, Bagavathiappan S, Jayakumar T, et al. Medical applications of infrared thermography: a review[J]. Infrared physics & technology, 2012, 55(4): 221–235.

[2] Bouzida N, Bendada A, Maldague X P. Visualization of body thermoregulation by infrared imaging[J]. Journal of Thermal Biology, 2009, 34(3): 120–126.

[3] Lahiri B B, Bagavathiappan S, Nishanthi K, et al. Infrared thermography based studies on the effect of age on localized cold stress induced thermoregulation in human[J]. Infrared Physics & Technology, 2016, 76: 592–602.

[4] Usamentiaga R, Fidanza A, Yousefi B, et al. Advancing knee injury prevention and anomaly detection in rugby players through automated processing of infrared thermography: A novel biothermodynamics approach[J]. Thermal Science and Engineering Progress, 2025: 103782.

[5] Lahiri B B, Bagavathiappan S, Philip J. Infrared thermal imaging based study of localized cold stress induced thermoregulation in lower limbs: The role of age on the inversion time[J]. Journal of thermal biology, 2020, 94: 102781.

[6] Liu Y, Yao Y, Wang F, et al. Review of unsupervised machine learning methods in active infrared thermography for defect detection and analysis[J]. Quantitative InfraRed Thermography Journal, 2025: 1–28. Doi: 10.1080/17686733.2025.2540662.

[7] Machado Á S, da Silva W, Lemos A L, et al. Impact of a low-intensity exercise prior to infrared thermography measurements on skin temperature under conditions of muscle soreness[J]. Scientific Reports, 2026, 16(1): 10380.

[8] Garcia Vargas I, Fernandes H. Spatial and temporal deep learning algorithms for defect segmentation in infrared thermographic imaging of carbon fibre-reinforced polymers[J]. Nondestructive Testing and Evaluation, 2026, 41(1): 45–65.

[9] Thapa D, Welch R, Dabas R P, et al. Comparison of long-wave and mid-wave infrared imaging modalities for photothermal coherence tomography of human teeth[J]. IEEE Transactions on Biomedical Engineering, 2022, 69(9): 2755–2766.

[10] Chang C H, Wang F, Sfarra S, et al. Efficient background removal and defect identification in infrared thermography of CFRP composites using adaptive fixed-rank kriging[J]. Measurement Science and Technology, 2026, 37(10): 105407.

[11] Kulkarni N N, Dabetwar S, Benoit J, et al. Comparative analysis of infrared thermography processing techniques for roadways' sub-pavement voids detection[J]. NDT & E International, 2022, 129: 102652.

[12] Fleuret J, Ebrahimi S, Castanedo C I, et al. On the use of pulsed thermography signal reconstruction based on linear support vector regression for carbon fiber reinforced polymer inspection[J]. Quantitative InfraRed Thermography Journal, 2023, 20(2): 39-61.

[13] Liu Y, Wang F, Liu K, et al. Deep convolutional autoencoder thermography for artwork defect detection[J]. Quantitative InfraRed Thermography Journal, 2024, 21(6): 367–383.

[14] Zhang Y, Xu C, Liu P, et al. One-dimensional deep convolutional autoencoder active infrared thermography: Enhanced visualization of internal defects in FRP composites[J]. Composites Part B: Engineering, 2024, 272: 111216.